Int. J. Electrochem. Sci., 14 **(2019)** 625 – 633, doi: 10.20964/2019.01.56

International Journal of
ELECTROCHEMICAL
SCIENCE
www.electrochemsci.org

Generation of Sn Whiskers During Electrodeposition

M. Saitou

University of the Ryukyus, Department of Mechanical Systems Engineering, 1 Senbaru Nishihara-cho Okinawa, 903-0213, Japan.
*E-mail: saitou@tec.u-ryukyu.ac.jp

Received: 1 September 2018 / *Accepted:* 26 October 2018 / *Published:* 30 November 2018

Sn whiskers generated during electrodeposition on a Cu plate within a range of the deposition temperature from 273 to 303 K were investigated using scanning electron microscopy and X-ray diffraction. The critical film thickness for the formation of Sn whiskers on a Sn thin film was determined (1.9 µm). The critical film thickness was found to be independent of the deposition temperature. At the film thicknesses more than 5 µm, the (220) dominant crystallographic plane transformed the (112) plane parallel to the Cu plate. This can be attributed to the morphological change (coarse to dense Sn whiskers). This suggests that the Sn whiskers with the (220) plane acted as crystal seeds to generate the Sn whiskers with the (112) plane. The fine string-like Sn whiskers generated at 303 K during the electrodeposition showed an anomalous growth rate of 45 nm s^{-1} at least.

Keywords: Sn whisker; Electrodeposition; Critical film thickness; Dominant crystallographic plane

1. INTRODUCTION

Sn whiskers are well known to grow spontaneously from Sn thin films on metal substrates in a normal environment and a long Sn whisker that makes a short circuit can easily destroys electrical systems. Various efforts have been made to investigate the mechanism underlying the formation of Sn whiskers [1–2]. However, these investigations could not explain an anomalous growth rate of Sn whiskers that have a maximum value of 100 nm s^{-1}. Recently, instead of conventional driving forces such as oxidation, recrystallization, and stress [3–4], a new model that takes into consideration the electrostatic energy gain in the electric field surrounding a Sn whisker [5] has been proposed. The quantitative predictions by the new model was consistent with experimental results about a growth rate and density of Sn whiskers formed on Sn thin films [6].

Sn thin films have recently gained immense attention as a promising anode material for lithium ion batteries owing to their low cost and high specific capacity [7–9]. However, Sn thin film anodes suffer from pulverization due to the huge volume changes induced by repeated the cycles of lithiation and delithiation processes. Therefore, to enhance the ability to decrease the stress induced during the lithiation and delithiation cycles, the structure of Sn thin films has been investigated extensively. For example, Sn thin films with three-dimensional ordered microporous structure [10] can potentially reduce the stress induced by lithiation and delithiation. Sn whiskers have a variety of shapes such as straight, helical, tangled, and kinked filaments or nodules [1], and voids between Sn whiskers facilitate the alleviation of the stress generated during the lithiation and delithiation processes.

We also reported that Sn whiskers on a Sn thin film were generated during electrodeposition and had a rod shape surrounding by crystallographic planes [11]. Sn thin films used for the formation of Sn whiskers are usually tested in a variety of environments after electrodeposition. The electrodeposition parameters affect the size and structure of Sn grains, which are characterized by their crystallographic planes and directions, which were reported to relate a Sn whisker density and structure generated on Sn films [12]. In this study, we report the Sn whisker formation not after electrodeposition but during electrodeposition.

The aims of the present study are to determine the critical film thickness at which Sn whiskers are formed on Sn thin films during electrodeposition, and to show the transition of the dominant crystallographic plane in Sn thin films corresponds to the changes in the morphology of the surface containing Sn whiskers.

2. EXPERIMENTAL SETUP

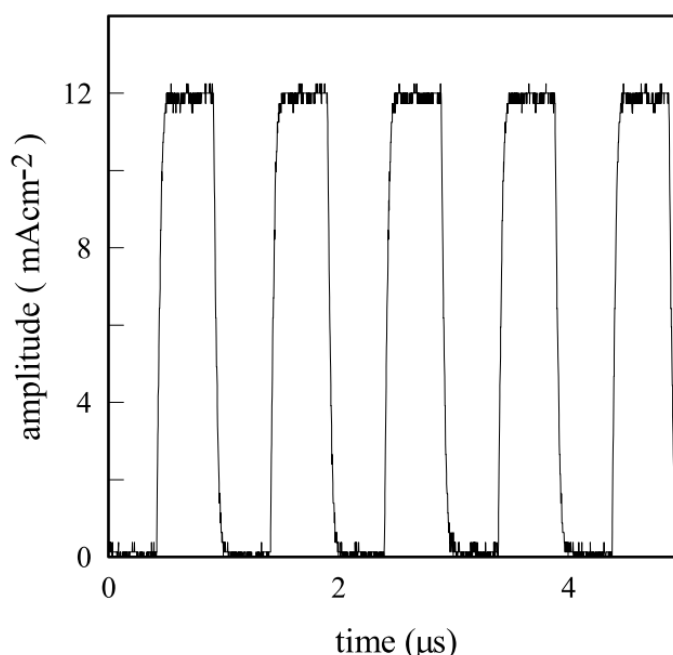

Figure 1. Rectangular pulse current with an amplitude of 12 mA cm^{-2} and a frequency of 1 MHz.

As the cathode and anode, a copper plate of 30×10 mm^2 (99.99 wt % purity) and carbon plate of 50×40 mm^2 were used, respectively. One side of the copper plate was electrically insulated. An aqueous solution including the following chemical compounds (mol L^{-1}) was prepared: $SnSO_4$ (0.8) and $KNaC_4H_4O_6 \cdot 4H_2O$ (0.55). The aqueous solution was strained with a membrane filter (pore size 0.1 µm) to remove tin hydroxide particles. The two electrodes were placed parallel to each other in an electrochemical cell filled with the aqueous solution maintained within a temperature range from 273 to 303 K during electrodeposition using a Peltier controller. A rectangular pulse current with a frequency of 1 MHz was supplied to the electrochemical cell by a function generator. A rectangular pulse current with an amplitude of 12 mA cm^{-2} was employed in all the experiments. A 22 Ω metal film resistor was connected in series with the electrochemical cell to calculate the current flowing to the electrochemical cell. Figure 1 shows the 1 MHz rectangular pulse current with an amplitude of 12 mA cm^{-2}.

After the electrodeposition, the Sn thin films (on the copper plate) were rinsed with distilled water and were then dried. The Sn thin films were weighted to a precision of 0.1 mg with an electric balance to calculate the thickness of the Sn thin film. The surface morphology of the Sn thin film was observed using a scanning electron microscope (SEM) (Hitachi TM3030). The crystallographic planes in the Sn thin film, which were parallel to the Cu plate, were examined using X-ray diffraction (XRD) (Rigaku Ultima) with CuKα radiation.

3. RESULTS AND DISCUSSION

3.1. Critical film thickness

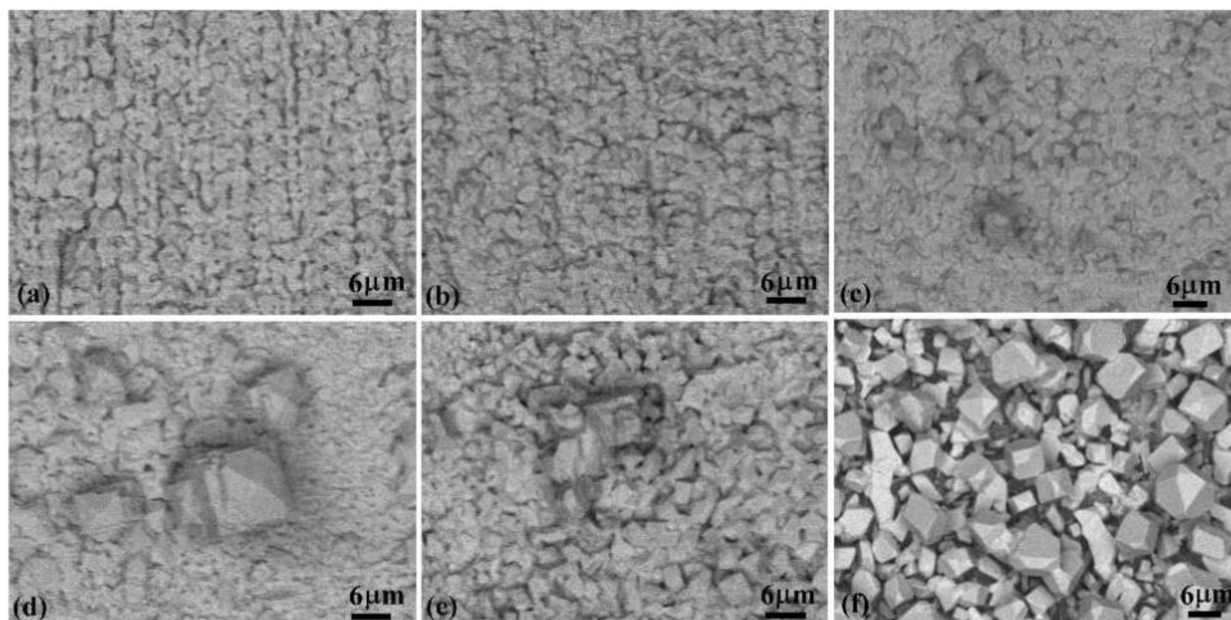

Figure 2. SEM images of the Sn thin films electrodeposited at 273 K. The films were (a) 1.4 µm , (b) 1.9 µm , (c) 3.4 µm , (d) 4.3 µm , (e) 5.3 µm , and (f) 7.4 µm thick.

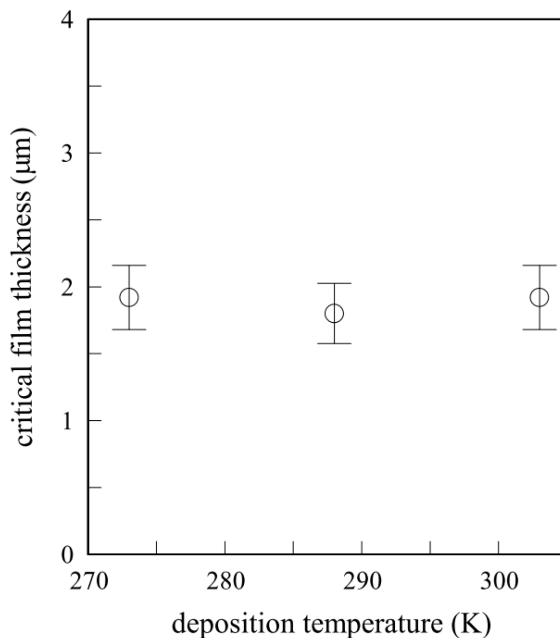

Figure 3. A plot of the critical film thickness vs. the deposition temperature.

The critical film thickness defined by the film thickness at which the Sn whisker formation occured was determined using SEM analysis. Figure 2 shows the typical SEM images of the Sn thin films with various film thicknesses, which were electrodeposited at a deposition temperature of 273 K. The SEM image of the Sn thin film in Fig. 2 (a) showed a rough surface on which some crystallographic planes appeared, however, no whisker embryo was observed. As the film growth proceeded, a Sn whisker embryo was observed at the film thickness of 1.9 μm in Fig. 2 (b). Thus, the critical film thickness was found to be 1.9 μm at a deposition temperature of 273 K. The whisker embryo, which was perpendicular to the Sn thin film, had a rod-like structure surrounded by crystallographic planes [11]. From Figs. 2 (c) and (d), it can be observed that the Sn whiskers with crystallographic planes were immensely grown. In the case of the thicker films in Figs. 2 (e) and (f), the Sn whiskers spread all over the Sn thin film surface and Sn whiskers with the height more than 30 μm were observed.

Figure 3 shows a plot of the critical film thickness vs. the deposition temperature. The critical film thickness independent of the deposition temperature indicates that the critical phenomenon was a non-thermal activation process. In heterogeneous film growth, a mismatch of the lattice constant between the substrate and the film grown layer-by-layer generates strain in the film [13]. The strain energy increases the free energy as the film thickness increases. To decrease the free energy, a transition from a smooth surface to a rough surface occurs. The rough surface increases the entropy and lessens the free energy. The critical film thickness using a kinetic Monte Carlo simulation [13] was estimated at several atomic layers, which is three orders of magnitude smaller than our experimental values. The whisker formation mechanisms reported previously [1–2] assumed that the strain energy causes the transfer of Sn atoms, which in turn reduces the strain energy. However, the fast transfer of Sn atoms even at temperatures as low as 273 K observed in this study needs to be explained. In addition, the internal stress in electrodeposited thin films is known to decrease with the film thickness [14].

According to the electrostatic theory proposed recently [5], the incubation time, t_o is given as

$$t_o = \frac{3\Lambda}{b\varepsilon E_0^2 h_o}, \quad (1)$$

where Λ is a constant, b is the mobility of Sn atom given by the Einstein relation, ε is the dielectric permittivity, E_o is the electric field strength, and h_o is the critical height over which the embryo of Sn whisker grows. The incubation time [15] is the time at which the height of the whisker embryo reaches h_o. In our experiment, the incubation time was 240 s and the critical film thickness became approximately 1.9 μm, which means the film thickness grown for 240 s. Substituting b~10^2 $cm^2s^{-1}J^{-1}$, h_o~10nm, Λ~1, and ε~1 [5] into Eq. (1), we have the electric field strength,

$$E_o \sim 2 \times 10^2\ V/cm. \quad (2)$$

Eq. (1) indicates that the incubation time, i.e., the critical film thickness is independent of the deposition temperature. This is consistent with the dependence of the critical film thickness on the deposition temperature as shown in Fig. 3.

3.2. XRD analysis of Sn thin films

The crystallographic planes in Sn thin films, which were parallel to the Cu plate, were investigated using XRD. Figure 4 shows the typical XRD patterns of the Sn thin films electrodeposited at 303 K. The XRD pattern of the Sn thin film with a thickness of 1.4 μm is shown in Fig. 4 (a).

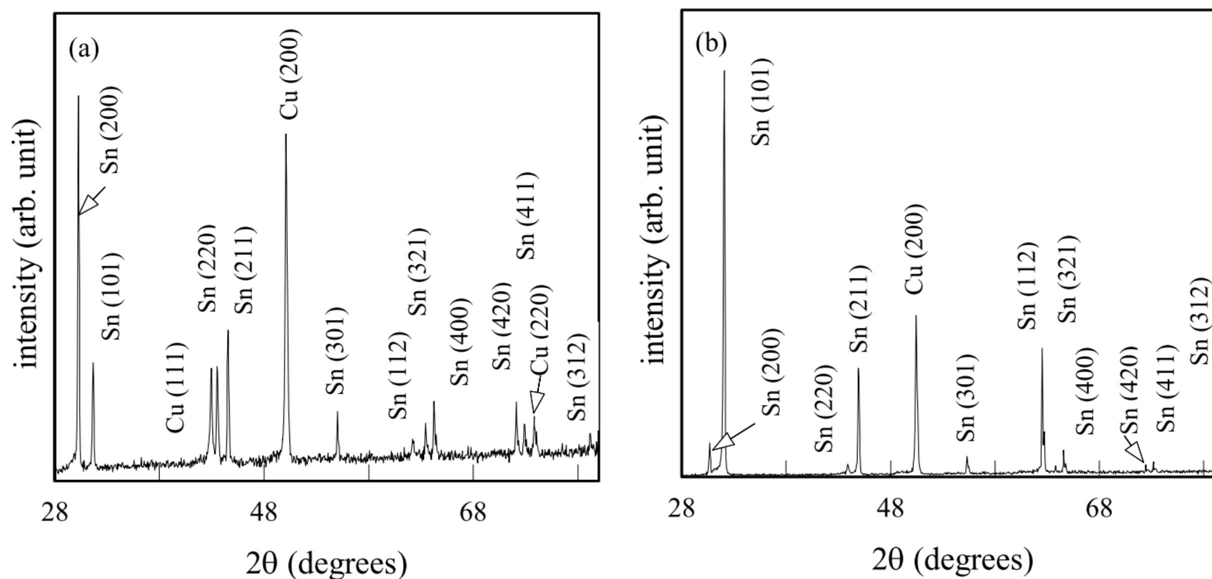

Figure 4. XRD patterns of the Sn thin films electrodeposited at 303 K. The Sn thin films were (a) 1.4 μm and (b) 9.6 μm thick.

Eleven diffraction peaks were indexed as β-Sn and the crystal structure of the thin film was concluded to be a tetragonal structure of β-Sn. The surface energies of crystallographic planes with low indices are the (110), (100) and (001) plane in descending order [16]. However, the diffraction peak from the (002) plane could not be observed [11]. This indicates that the Sn thin films did not show the surface energy minimum. In Fig. 4 (b), the XRD pattern of the Sn thin film with a thickness of 9.6 μm is shown.

Eleven diffraction peaks of β-Sn were shown. The diffraction peaks from the (200) and (220) plane significantly decreased in comparison with those in Fig. 4 (a). This suggests that a change in the diffraction intensity can be attributed to the formation of Sn whiskers.

To investigate the dominant crystallographic planes in the Sn thin films, which were parallel to the Cu plate, the texture coefficients T (hkl) [17] were defined as

$$T(hkl) = \frac{I(hkl)_i / I_o(hkl)_i}{\sum_N I(hkl)_i / I_o(hkl)_i}, \qquad (3)$$

where $I(hkl)_i$ is the measured intensity of the (hkl) diffraction, $I_o(hkl)_i$ is the standard intensity of polycrystalline Sn [18], and N is the total number of diffraction peaks. To determine the value of $I(hkl)_i$, a Gaussian function was used as a fitting function [17].

Figure 5 shows the plots of the texture coefficients of the Sn thin films formed at of 273, 288, and 303 K. Five crystallographic planes were chosen because their diffraction intensities were higher among the eleven diffraction planes. In Fig. 5 (a), the texture coefficients of the Sn thin films formed at 273K are shown.

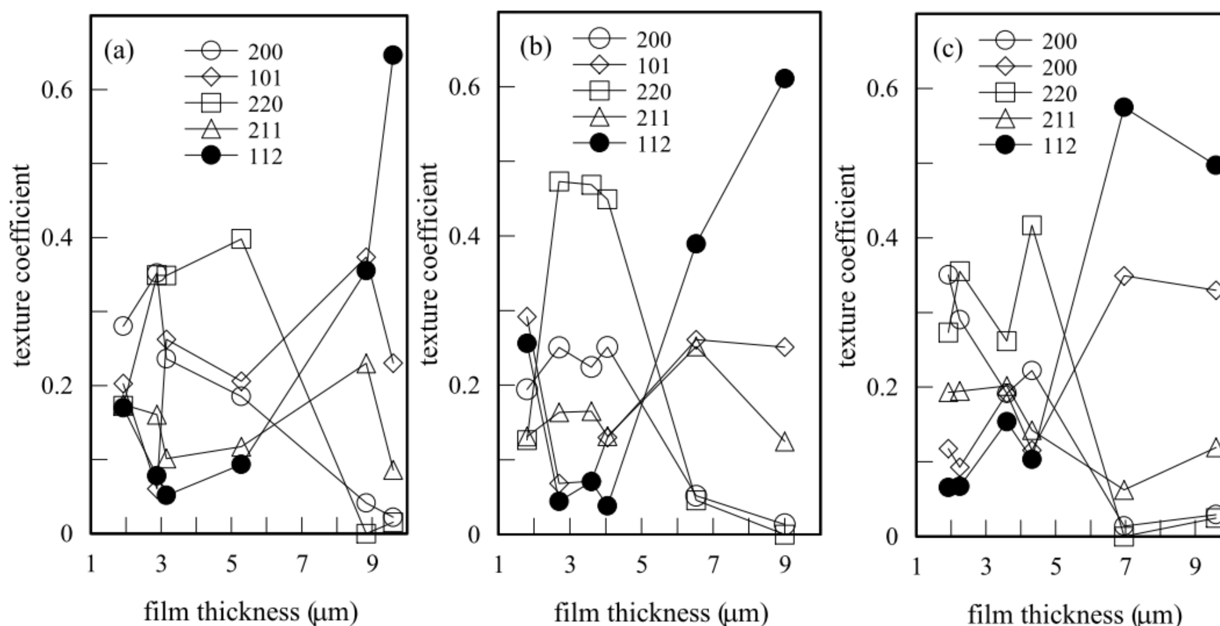

Figure 5. Plots of the texture coefficient vs. the film thickness for the Sn thin films electrodeposited at (a) 273, (b) 288, and (c) 303 K.

The texture coefficient, T(220) increased with the film thickness, and became dominant among the remaining texture coefficients. However, T(220) decreased at the film thickness of about 5 μm and became almost zero at the film thickness of 9 μm. On the other hand, the value of T(112) was very small at the film thicknesses less than 5 μm. However, the value of T(112) abruptly increased at the film thickness more than 5 μm and became about 0.65. This indicates that a transition of the dominant crystallographic plane from the (220) to the (112) plane occurred in the Sn thin film. Many Sn whiskers in Fig. 2 (f) had the (112) planes parallel to the Cu plate. In Fig. 5 (b), the texture coefficients of the Sn thin film formed at 288 K are shown. The dependence of T(220) and T(112) on the film thickness was

similar to that at 273K. In Fig. 5 (c), the texture coefficients of the Sn thin films formed at 303 K are shown. All the texture coefficients had the same tendency of those at 273 K and 288 K. The transition of the dominant texture coefficient from the (220) to the (112) plane was found to be independent of the deposition temperature.

Preferred crystallographic directions of Sn whiskers that grew for several days in a normal environment (room temperature and humidity) were reported to be <100>, <101>, and <111> directions [19]. As shown in Fig. 5, the (220) plane was dominant when the film thickness was thinner than 5 μm. Hence, the crystallographic direction of the Sn whiskers was <110> if the Sn whisker was perpendicular to the (220) plane. This is consistent with the direction of the Sn whisker formed in the normal environment after electrodeposition. When the film thickness was thicker than 5 μm, the (112) plane was dominant. Hence, the crystallographic direction of the Sn whisker was <3 3 11> if the Sn whisker was perpendicular to the (112) plane.

3.3. Anomalous increase in the number of Sn whiskers

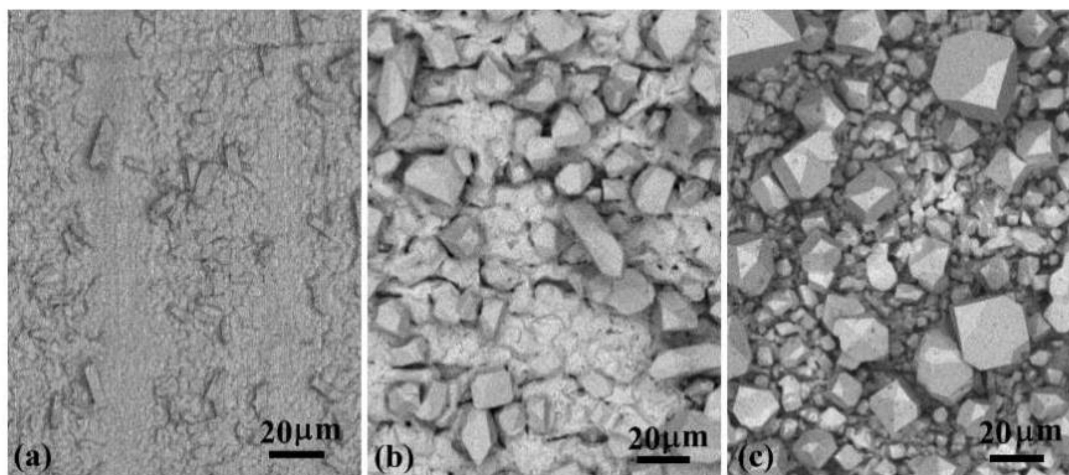

Figure 6. SEM images of the Sn thin films electrodeposited at 288 K. The films were (a) 4.3 μm , (b) 7 μm , and (c) 9.6 μm thick.

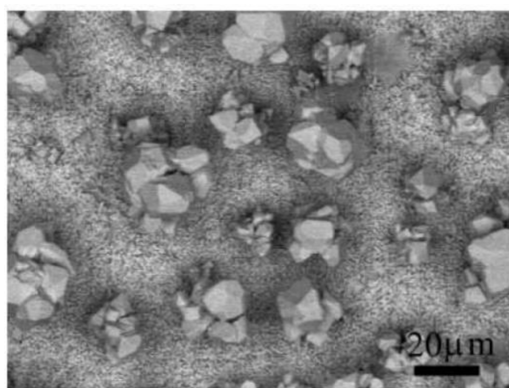

Figure 7. SEM images of the Sn thin film electrodeposited at 273 K. The Sn thin film was 9.6 μm thick.

Figure 6 shows the SEM images of Sn whiskers formed at 288 K. The number of Sn whiskers extremely increases with the film thickness. The anomalous increase in the number of Sn whiskers [20–21] can be attributed to a transition of the dominant crystallographic plane from the (220) to the (112) plane as shown in Fig. 5. In Fig. 6 (c), the Sn thin film was completely covered with the Sn whiskers. This suggests that the Sn whiskers with the (220) plane may act as seed crystals for the formation of the Sn whiskers with the (112) plane. In fact, as shown in Fig. 7, several Sn whiskers coalesced into one big Sn whisker.

3.4. String-like Sn whisker electrodeposited at 303 K

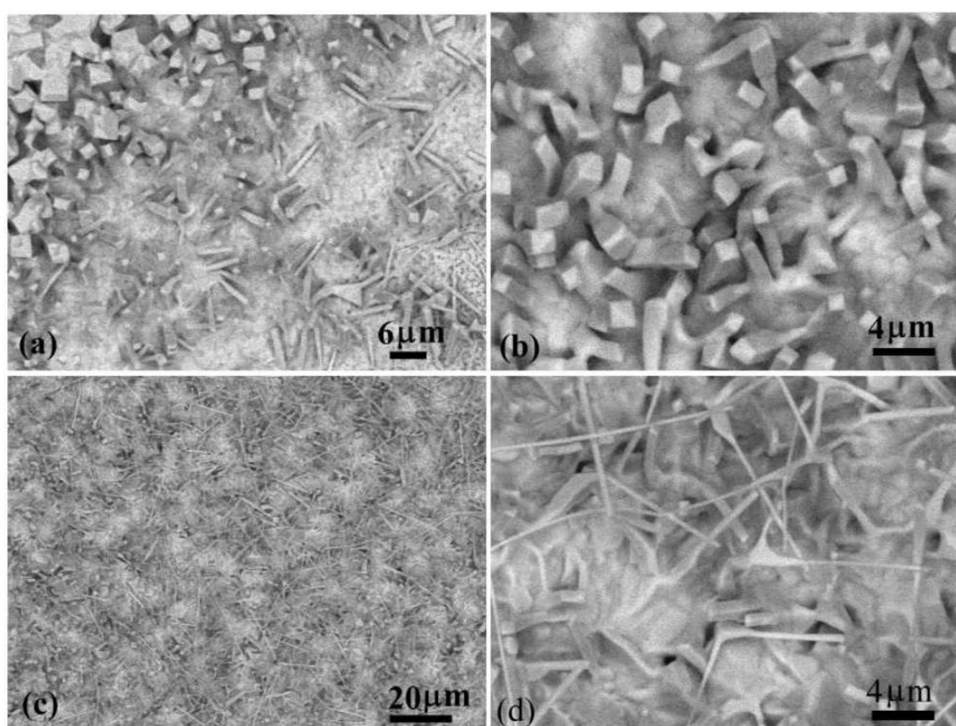

Figure 8. SEM images of Sn whiskers. The deposition temperatures and film thicknesses were 288 K and 7 μm for (a) and (b), and 303 K and 9.6 μm for (c) and (d).

Figure 8 shows the SEM images of the string-like Sn whiskers formed at 303K. With an increase in the film thickness, a variety of shapes in Sn whiskers appeared. In Figs. 8 (a) and (b), thick string-like Sn whiskers protruded from the Sn film surface.

In Fig. 8 (c) and (d), fine string-like Sn whiskers were grown parallel to the Sn film from thick string-like Sn whiskers. The length of the fine string-like Sn whisker increased by 30 μm within a deposition time of 660 s. The lowest growth rate of the fine string-like Sn whisker was approximately 45 nm s^{-1}, which is anomalous in comparison with the growth rate stated in the Ref. [1]. The growth directions of the fine string-like Sn were <110>, <201>, or <021> if the fine string-like Sn whisker was parallel to the (112) plane.

4. CONCLUSIONS

The critical film thickness at which a Sn whisker embryo is generated on the Sn thin film during electrodeposition was estimated at approximately 1.9 µm. The critical film thickness was independent of the deposition temperature, which was interpreted as the film thickness grown during the incubation time. The dominant crystallographic plane of the Sn thin films with the film thickness more than approximately 5 µm changed from the (220) to the (112) plane. The transition of the dominant crystallographic plane can be attributed to the morphological changes in the surface (the coarse Sn whiskers to the dense Sn whiskers). This suggests that Sn whiskers with the dominant plane (220) acted as crystal seeds to generate the Sn whiskers with the dominant plane (112). The string-like whiskers with the thickness more than 30 µm were observed at the deposition temperature of 303 K. The lowest growth rate was approximately 45 nms^{-1}.

References

1. P. Zhang, Y. Zhang, and Z. Sun, *J. Mater. Sci. Technol.*, 31 (2015) 675.
2. E. Chason, N. Jadhav, F. Pei, E. Buchovecky, and A. Bower, *Prog. Sur. Sci.*, 88 (2013) 103.
3. F. Pei, E. Buchovecky, A. Bower, and E. Chason, *Acta Mater.*, 129 (2017) 462.
4. F. Yang and Y. Shi, *Phys. Lett. A*, 381 (2017) 2767.
5. A. C. Vasko, C. R. Grice. A. D. Kostic, and V. G. Karpov, *MRS Commun.*, 5 (2015) 619.
6. V. G. Karpov, *Phys. Rev. Appl.*, 1 (2014) 044001.
7. H. Wang, X. Shi, K. Ding, C. Li, Y. Sun, H. Wang, H. Dou, and J. Pan, *Int. J. Electrochem. Sci.*, 13 (2018) 7718.
8. B. Wang, B. Luo, X. Li, and L. Zhi, *Mater. Today*, 15 (2018) 544.
9. H. Tian, F. Xin, X. Wang, W. He, and W. Han, *J. Materiomics*, 1 (2015) 153.
10. E. M. Sorensen, S. J. Barry, H-K Jung, J. R. Rondineli, J. T. Vaughey, and K. Poeppelmeier, *Chem. Mater.,* 18 (2006) 482.
11. M. Saitou, *Int. J. Electrochem. Sci.*, 13 (2018) 1869.
12. M. A. Ashworth, G. D. Wilcox, R. L. Higginson, R. J. Heth, C. Liu, and R. J. Mortimer, *Microelectron. Reliab.*, 55 (2015) 180.
13. A. Baskaran and P. Smerek, *J. Appl. Phys.*, 111 (2012) 044321.
14. M. Saitou, S. Oshiro and Y. Sagawa, *J. Appl. Phys.*, 104 (2008) 093518.
15. D. Susan, J. Michael, R. P. Grant, B. Mckenzie, and W. G. Yelton, *Metall. Mater. Trans. A*, 44A (2013) 1485.
16. L. Vitos, A.V. Ruban, H. L. Skriver, and J. Kollár, *Surf. Sci.*, 411 (1998) 186.
17. M. Saitou, *Int. J. Electrochem. Sci.*, 11 (2016) 6491.
18. H. E. Swanson and E. Tatge, *Standard X-ray diffraction Powder Patterns*, NBS Circular 539, Vol. 1 (1953).
19. J. Stein, U. Welzel, A. Leineweber, W. Huegel, and E. J. Mittemeijer, *Acta Mater.*, 86 (2015) 102.
20. M. W. Barsoum and L. Farber, *Science*, 284 (1999) 937.
21. T. Fang, M. Osterman, and M. Pecht, *Microelectron. Reliab.*, 46 (2006) 846.

© 2019 The Authors. Published by ESG (www.electrochemsci.org). This article is an open access article distributed under the terms and conditions of the Creative Commons Attribution license (http://creativecommons.org/licenses/by/4.0/).